2. BACKGROUND

Particulate Nitrate Formation

Particulate nitrate derives from emissions of nitrogen oxides (NO_x), but in a highly nonlinear manner. Gas-phase oxidation of NO_2 yields nitric acid (HNO_3); aqueous-phase reactions are by comparison unimportant (Seinfeld and Pandis, 1998). During daytime, HNO_3 is produced by reaction of NO_2 with hydroxyl radical (OH):

$$OH + NO_2 \rightarrow HNO_3 \quad (R1)$$

At night, the following reactions become relatively more important:

$$O_3 + NO_2 \rightarrow NO_3 + O_2 \quad (R2)$$

$$NO_2 + NO_3 \leftrightarrow N_2O_5 \quad (R3,R4)$$

$$N_2O_5 + H_2O \rightarrow 2\ HNO_3 \quad (R5)$$

The rate of nitric acid production, via reactions R1 through R5, is a nonlinear function of NO_x concentration (Meng et al., 1997). When R1 is limited by OH radical concentrations, decreases in the nonlimiting reactant, NO_2, will not decrease the rate of HNO_3 formation until NO_2 becomes limiting. Reaction R1 becomes limited by radical concentrations as NO_x concentrations increase (Sillman, 1995), but whether the limiting reactant in reaction R1 is OH radical or NO_2 depends upon the rates of emissions of NO and NO_2, the rate of conversion of NO to NO_2, and the rates of production and destruction of OH (Seinfeld and Pandis, 1998). Reaction R1 is a sink for OH radical, whereas the competing reaction of OH with hydrocarbon species (RH) regenerates OH radical (Sillman, 1995):

$$RH + OH + O_2 \rightarrow RO_2 + H_2O \quad (R6)$$

$$RO_2 + NO + O_2 \rightarrow R'CHO + HO_2 + NO_2 \quad (R7)$$

$$HO_2 + NO + O_2 \rightarrow OH + NO_2 \quad (R8)$$

The ratio of hydrocarbon species concentrations to NO_x concentrations is therefore a key determinant of which reactant in R1 limits the rate of production of nitric acid.

When reaction R1 is NO_2 limited, decreases in NO_x may be expected to decrease the rate of formation of HNO_3, and, depending upon other factors, may also decrease the ambient concentrations of particulate nitrate. Conversely, when R1 is radical limited, decreases in VOC may decrease the rate of formation of HNO_3. However, it is also possible under radical limited conditions for decreases in VOC to increase HNO_3 levels. This opposing effect may occur when reaction R1 is dominated by the reaction of NO_2 with a radical species derived from either acetaldehyde or acetone to form peroxyacetyl nitrate (PAN):

$$CH_3C(O)O_2 + NO_2 \text{ <--> } CH_3C(O)O_2NO_2 \quad (PAN) \qquad (R9,R10)$$

The reverse reaction (R10) has a strong temperature dependence, so that thermal decomposition of PAN can regenerate NO_2. If VOC reductions shift the fate of NO_2 from PAN production (R9) to HNO_3 formation (R1), increases in particulate nitrate concentrations may occur (Meng et al., 1997). However, if R1 is dominant and limited by radical concentrations, further reduction of radical levels through VOC reductions may be expected to decrease HNO_3 formation.

Nitric acid and ammonia (NH_3) establish the following equilibrium:

$$HNO_3\ (g) + NH_3\ (g) \text{ <-> } NH_4NO_3\ (p) \qquad (R11, R12)$$

where "g" and "p" denote the gas and particulate phases, respectively. The formation of particulate nitrate via reaction R11 may be limited by the concentrations of either HNO_3 or NH_3 (Watson et al., 1994; Ansari and Pandis, 1998). Ammonia concentrations, in turn, are affected by concentrations of sulfuric acid (H_2SO_4) and bisulfate (HSO_4^-) via dissociation of aqueous H_2SO_4 and reaction of bisulfate or sulfate with NH_3:

$$H_2SO_4\ (a) \text{ <-> } H^+ + HSO_4^- \qquad (R13, R14)$$

$$HSO_4^- \text{ <-> } H^+ + SO_4^{2-} \qquad (R15, R16)$$

$$SO_4^{2-} + NH_3\ (g) \text{ <-> } (NH_4)_2SO_4 \qquad (R17, R18)$$

$$HSO_4^- + NH_3\ (g) \text{<-> } (NH_4)HSO_4 \qquad (R19, R20)$$

Ammonia may become limiting in reaction R11 because NH_3 reacts preferentially with H_2SO_4 or HSO_4^- aerosol to form either $(NH_4)_2SO_4$ or NH_4HSO_4 (R17 and R19). Reductions of SO_2, while resulting in decreases of aerosol sulfate, can then lead to increases in particulate nitrate, as the ammonia freed by the reverse reactions R18 and R20 becomes available to react with HNO_3 in R11.

Sodium nitrate may also be generated via reaction of nitric acid with sodium chloride in marine aerosol (Martens et al., 1973; Wexler and Seinfeld, 1992; Gard et al., 1998). Whereas ammonium nitrate is typically found in the fine ($PM_{2.5}$) aerosol fraction, sodium nitrate is more likely to occur in the coarse fraction ($PM_{2.5}$ to PM_{10}) (Ottley and Harrison, 1992; Finlayson-Pitts and Pitts, 1986).

The complexity of these reaction paths indicates that simple correlations between ambient concentrations of, e.g., NO_x and particulate nitrate are unlikely to be observed. Modeling studies

(which explicitly incorporate the reactions outlined above) to date have provided varied results. Pun and Seigneur (2001) used a box model centered on an urban location in the San Joaquin Valley to show that particulate nitrate levels were radical limited and more responsive to VOC than to NO_x reductions. In contrast, Fujita et al. (2000) found that winter particulate nitrate concentrations in rural portions of the San Joaquin Valley would be responsive to NO_x reductions. For Los Angeles, Meng et al. (1997) modeled a summer day (August 28, 1987) from the Southern California Air Quality Study (SCAQS) and found that VOC reductions led to increases of $PM_{2.5}$, primarily through the shift from PAN to HNO_3 production discussed above.

Gas-phase Reactions: HNO_3 Production

In previous unpublished work, we carried out box-model simulations to identify measurable species whose values are capable of characterizing the response of HNO_3 (and, hence, of total nitrate) to NO_x reductions. It was found that differences in HNO_3 concentrations can be related to how NO_x-rich or NO_x-poor a system is. These simulations are useful for understanding the general relations between concentrations of HNO_3 and other species. They are not a representation of nitric-acid formation in a specific actual situation, although a location and date had to be specified to run the simulations.

The simulations were carried out for latitude 37.75N and longitude 122.22W (Oakland airport) with radiation for clear sky conditions on December 21. All simulations were initiated at 6:00 a.m. PST and continued for 24 hours. Constant temperature (283K) was used throughout each simulation. VOC composition characteristic of average urban conditions was used for all simulations.

Six sets of 100 photochemical box-model simulations were carried out as listed in Table 1. Two chemical mechanisms were used: the carbon bond 4 (CB4) and the Carter-Atkinson-Lurmann-Lloyd (CALL) (Lurmann et al., 1986) mechanisms. Three types of conditions were investigated for each of the two chemical mechanisms. In the first, the emissions were input entirely at the start of the simulation and mixing heights remained fixed at 300 m throughout. Since the simulations were carried out using a box model, no distinctions were made between point, area, and mobile-source emissions.

In the second set of conditions, time-varying emissions inputs and mixing heights were used and nonzero deposition velocities were assigned to ozone, NO_2, and HNO_3. For these conditions, 40 percent of the emissions were input between the hours of 6:00 and 9:00 a.m., 30

percent from noon through 2:00 p.m., and 30 percent from 4:00 through 6:00 p.m. Mixing heights were varied from 300 to 800 m over the period 8:00 a.m. to 1:00 p.m. and were then reduced to 300 m by 6:00 p.m. A constant deposition velocity of 0.1 cm s^{-1} was used for ozone, NO_2, and HNO_3. (This value is low for HNO_3. However, under the winter conditions simulated, and provided sufficient ammonia was present, over 90 percent of the HNO_3 would be converted to aerosol nitrate, most of which would be expected to exist on particles having aerodynamic diameters on the order of one micron or less. For such particles, a deposition velocity of about 0.1 cm s^{-1} is appropriate).

The third set of conditions was identical to the second set but also included the presence of aloft concentrations of 0.03 ppmv CO, 0.002 ppmv NO, 0.005 ppm NO_2, 0.007 ppmv O_3, 0.0015 ppmv PAN, and 0.0015 ppmv HNO_3. These values were selected to represent a partially aged air mass having concentrations within the range of those generated by the simulations. The box model's capabilities are limited to simulations of 24 hours or less, so more realistic situations corresponding to multi-day pollution episodes could not be studied.

Within each of the six sets, 100 simulations were conducted by varying the VOC and NO_x emissions inputs each over one order of magnitude. For the simulations having an initial charge of pollutants, the input VOC concentrations ranged from 0.1 to 1.0 ppmC and the input NO_x concentrations varied from 0.01 to 0.1 ppmC; for other simulations, the total masses of the time-dependent emission inputs summed to the equivalent masses of the listed initial VOC and NO_x concentrations.

Table 1. Conditions used for six sets of 100 photochemical box-model simulations.

Characteristic	Values Used	
Location	37.75°N and 122.22°W	
Date	December 21	
Temperature	283°K	
Mechanism	CB4 or CALL	
Duration	24 hours	
Temporal emissions profile	Initial loading	40% 6:00 to 9:00 a.m., 30% noon to 2:00 p.m., 30% 4:00 to 6:00 p.m.
Mixing height	300 m	300 to 800 m
Deposition velocity	zero for all species	0.1 cm s^{-1} for O_3, NO_2, and total nitrate
Aloft concentrations	zero for all species	0.03 ppmv CO, 0.002 ppmv NO, 0.005 ppm NO_2 , 0.007 ppmv O_3, 0.0015 ppmv PAN, 0.0015 ppmv HNO_3

Since six-hundred individual simulations were carried out, the results could not be examined individually. Instead, 24-hour mean concentrations of approximately 20 species were determined for each simulation (the 24-hour means were used to reflect the temporal resolution of the 24-hour PM standards). The results are most easily depicted using EKMA-style plots, as shown in Figure 1 for HNO_3 concentrations as a function of the VOC and NO_x inputs. This figure shows that the response of HNO_3 to precursor reductions is dependent on the ratio of VOC/NO_x as well as upon the absolute concentrations of VOC and NO_x. HNO_3 levels decrease with decreasing NO_x inputs at higher VOC/NO_x ratios (lower right corner of Figure 1), but may increase at lower VOC/NO_x ratios (upper right corner of Figure 1). In contrast, HNO_3 levels decrease with decreasing VOC inputs at lower VOC/NO_x ratios (upper right corner of Figure 1), but may increase at higher VOC/NO_x ratios (lower right corner of Figure 1). HNO_3 levels decrease more rapidly in response to decreasing VOC at higher VOC concentrations (upper right) than at lower VOC concentrations (upper left). Over much of the domain shown, the isopleths are near-vertical or near-horizontal. In many situations, therefore, reductions of either VOC alone (horizontal isopleths) or NO_x alone (vertical isopleths) may not change particulate nitrate concentrations by measurable amounts.

In contrast with the HNO_3 isopleths, contours for PAN and for ozone both bend sharply (they are not L-shaped) (Figures 2 and 3). Therefore, in many situations the reduction of NO_x concentrations is predicted to increase PAN or ozone concentrations. This strong counterdirectional response of PAN and ozone contrasts with the response of HNO_3 to NO_x changes: the HNO_3 response is more likely to be a lack of change, rather than a counterdirectional change.

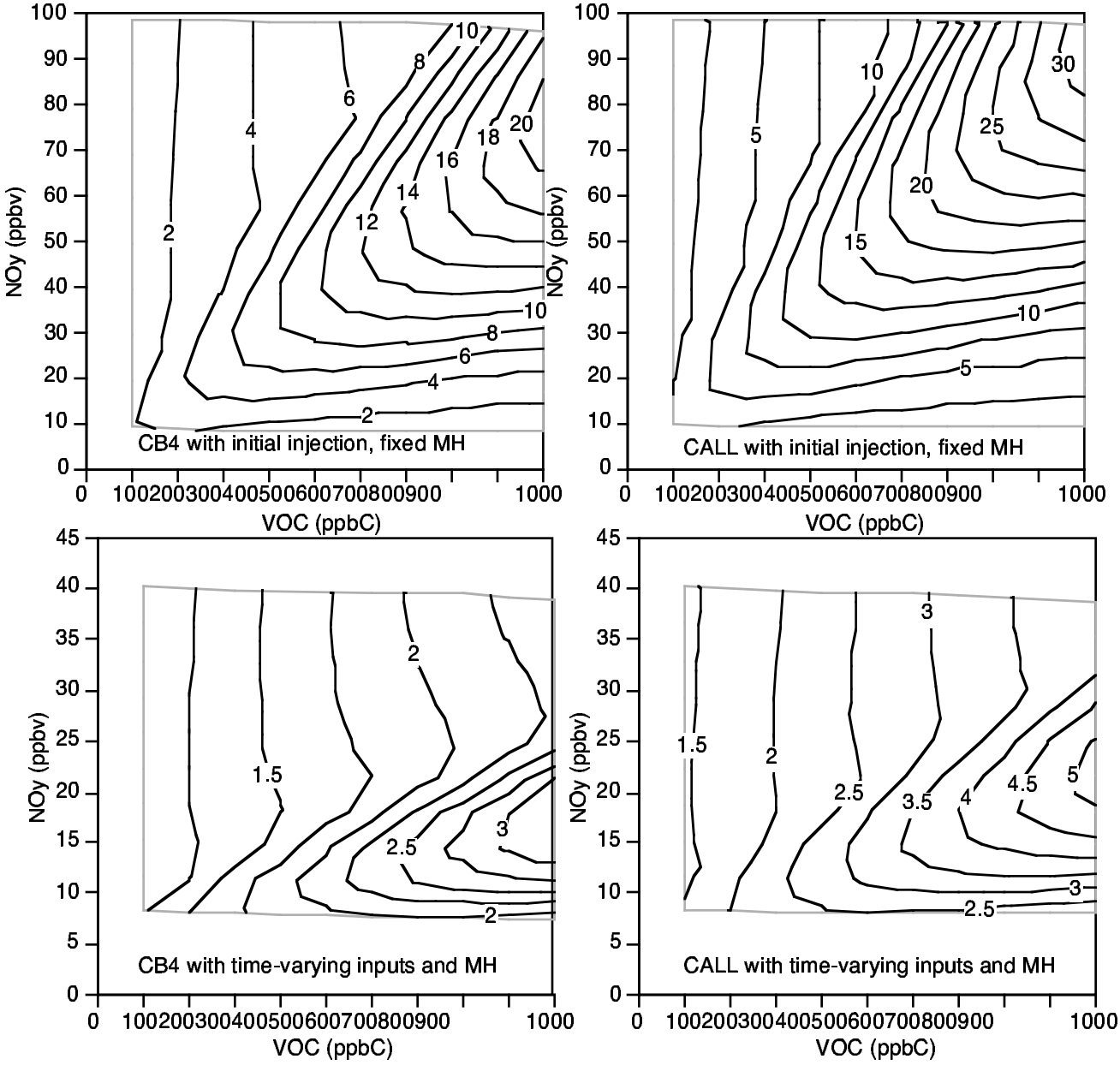

Figure 1. Gas-phase box-model simulations showing HNO_3 isopleths calculated using OZIPR for December 21, 37N, clear sky conditions.

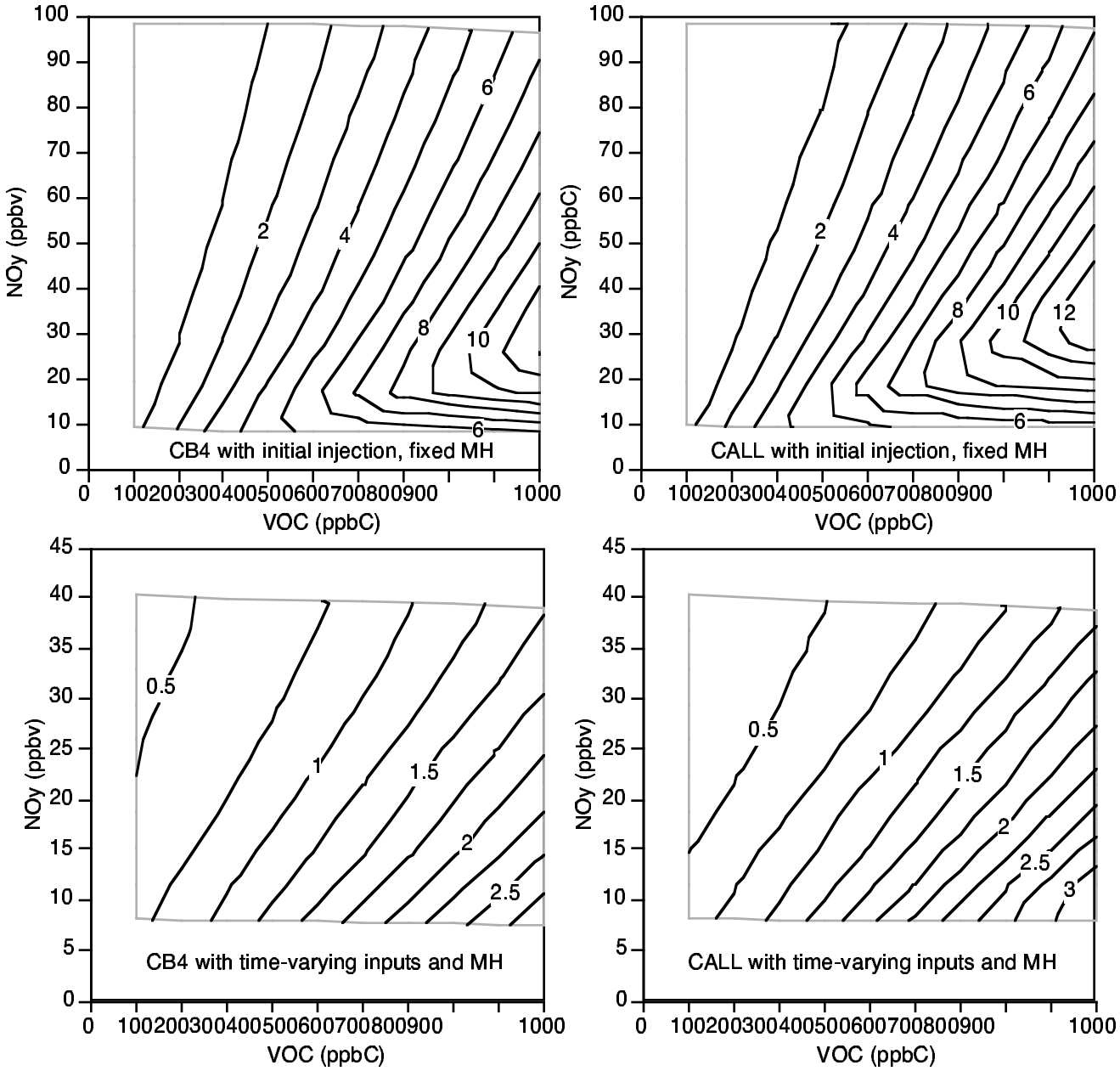

Figure 2. Gas-phase box-model simulations showing PAN isopleths calculated using OZIPR for December 21, 37N, clear sky conditions.

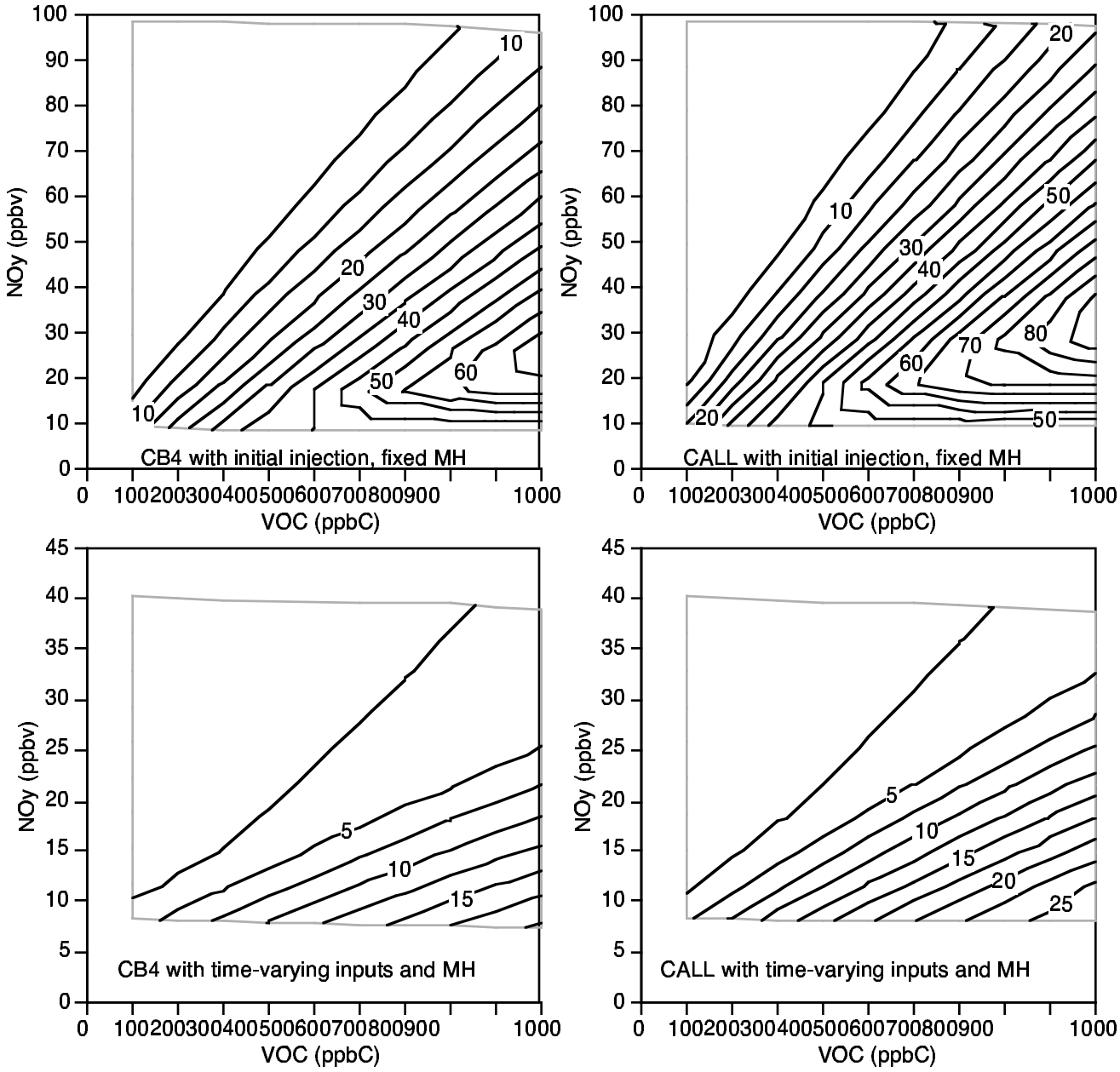

Figure 3. Gas-phase box-model simulations showing 24-hour ozone isopleths calculated using OZIPR for December 21, 37N, clear sky conditions.

Gas-Particle Equilibrium

Thermodynamic equilibrium models, when applicable, provide a useful description of relations between particulate ammonium nitrate and its gas-phase precursors, ammonia and nitric acid. In addition, equilibrium models can describe the effects of changes in sulfate concentrations on nitrate concentrations. Under some circumstances, though, particulate nitrate and its precursors may be too far from equilibrium for equilibrium models to be even approximately correct. Therefore, the adequacy of the approximation should be checked when applying an equilibrium model.

If thermodynamic equilibrium is an adequate approximation, model simulations show when particulate nitrate will respond to changes in HNO_3 and when it will not (Figure 4). At lower concentrations of ammonia and higher concentrations of HNO_3 or of sulfate, particulate nitrate formation is limited by the available ammonia. Particulate nitrate concentrations then decrease if ammonia concentrations decrease. They increase if sulfate concentrations decrease, and do not change if HNO_3 concentrations decrease (Figure 4).

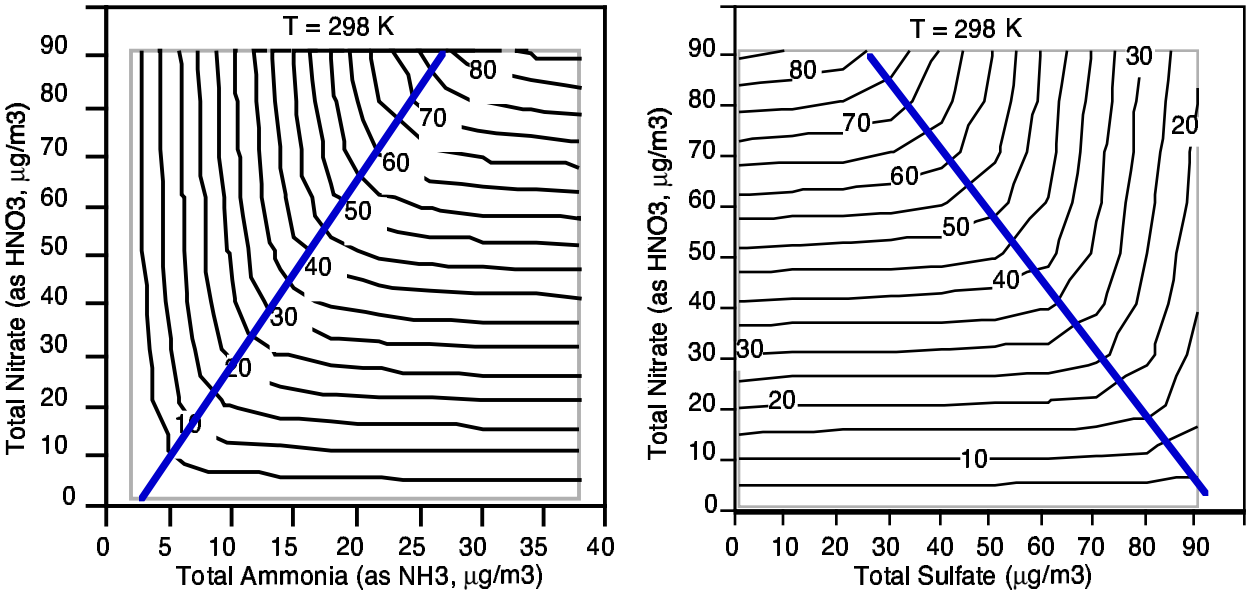

Figure 4. Predicted particulate nitrate concentrations as a function of variations in total nitrate and total ammonia (left panel) or sulfate (right panel). The straight line delineates the points at which total ammonia is equal to total nitrate plus sulfate (molar basis times charge, or equivalents), adjusting for other inorganic species according (see text). It marks a transition between a region where particulate nitrate responds to changes in HNO_3 (below the line) and where it does not (above the line). The region above the line is ammonia limited and has total ammonia concentrations less than the sum of sulfate and total nitrate (equivalents). Source: Blanchard et al. (2000).

The nitrate response that is predicted by thermodynamic equilibrium models has been classified into two or more categories using the values of measurable species. One such parameter is excess ammonia, defined as (Blanchard et al., 2000):

$$\text{Excess ammonia} = [NH_3\ (g)] + [NH_4^+\ (p)] - 2\ [SO_4^{2-}\ (p)] - [NO_3^-\ (p)] - [HNO_3\ (g)] - [HCl\ (g)] + 2\ [Ca^{2+}] + 2\ [Mg^{2+}] + [Na^+] + [K^+] - [Cl^-] \quad (1)$$

where all concentrations are in units of μmol m^{-3}, and "g" and "p" denote gas and particle phases, respectively. The set of values for which excess ammonia is zero yields the straight lines demarking the transitions between ammonia and HNO_3 limitation shown in Figure 4. Under many circumstances, principally for measurements of fine particles, the species shown in the second row of Equation 1 may be neglected because their concentrations are low. The L-shaped contours shown in Figure 4 permit a two-way division of samples into those that are ammonia-limited and those that are HNO_3 limited. However, the contours deviate from the sharp L shapes at higher temperatures and lower relative humidities (e.g., T>298K and RH<80 percent) and at lower temperatures combined with higher relative humidities (T<293K and RH>90 percent). Where the contours are rounded at the transition, or where the isolines deviate more from near-horizontal or near-vertical, the response of particulate nitrate can be more complex and less easily classified into only two categories.

Ansari and Pandis (1998) classify nitrate changes into four general outcomes using the gas ratio, defined as the ratio of free ammonia to total nitrate:

$$\text{Gas ratio} = NH_3^F / HNO_3^T \quad (2)$$

where $NH_3^F = [NH_3\ (g)] + [NH_4^+\ (p)] - 2\ [SO_4^{2-}\ (p)]$

and $HNO_3^T = [NO_3^-\ (p)] + [HNO_3\ (g)]$ (molar units)

A gas ratio of one corresponds to excess ammonia of zero (Equation 1, first line only), so that a gas ratio near one (0.4 to 1.5, depending on temperature and RH) delineates a transitional region with nonlinear responses. At higher ratios, ammonia is present in excess and particulate nitrate decreases in response to HNO_3 reductions. At lower ratios (0 to 0.4), ammonia is limiting and particulate nitrate does not decrease in response to HNO_3 reductions, and increases in response to sulfate decreases. Very low gas ratios (< 0) are acidic samples for which ammonia is so limiting that particulate nitrate concentrations are very low.

Blanchard et al. (2000) characterized ammonia limitation of particulate nitrate formation using three sets of data from California locations. The principal finding was that ammonia did not limit nitrate formation in most samples (Figure 5).

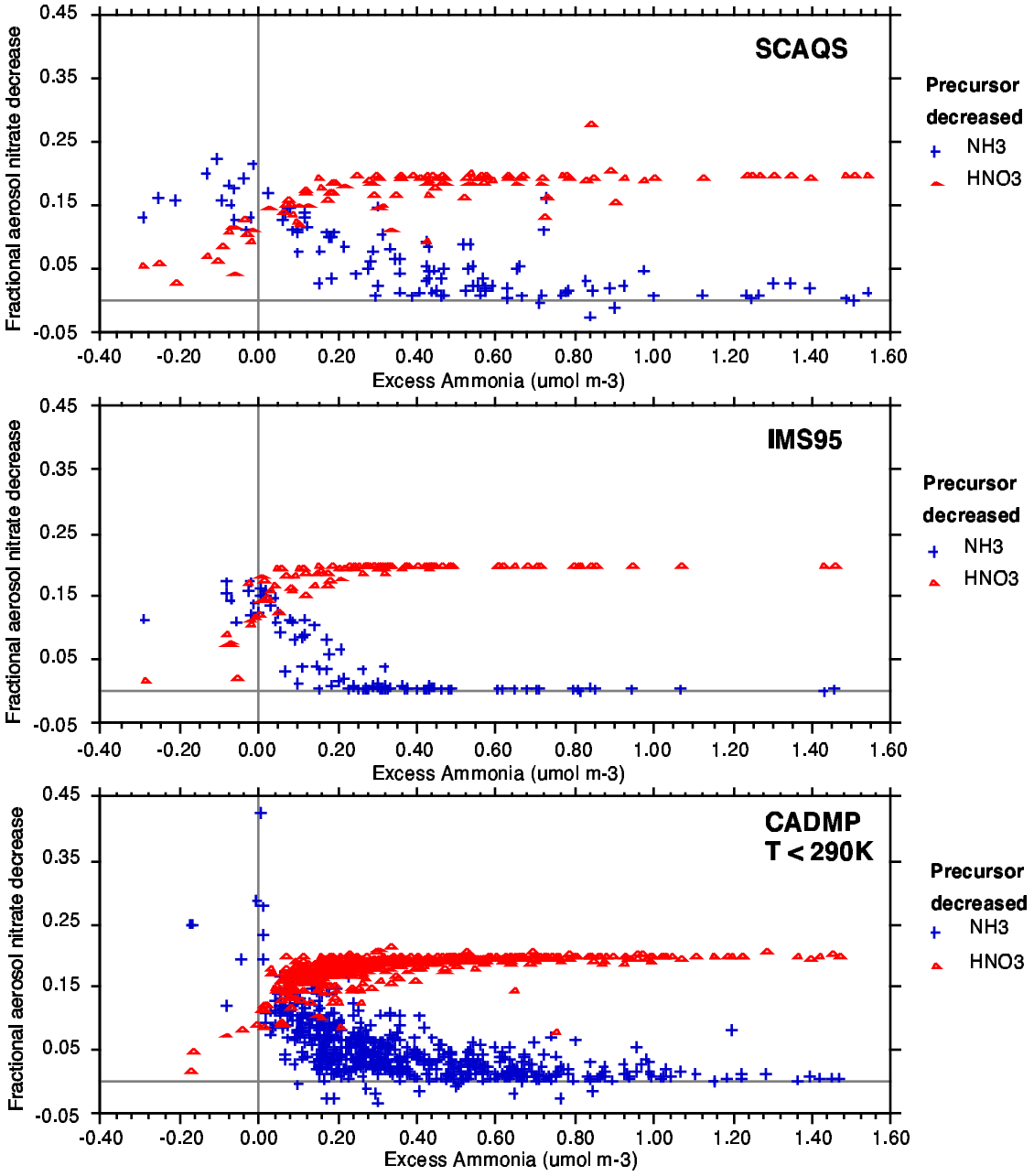

Figure 5. Predicted response of particulate nitrate to reductions of NH_3 or HNO_3 using three data sets (SCAQS, IMS95, and CADMP). The fractional decrease was computed relative to the base case nitrate concentrations. Source: Blanchard et al. (2000).

As shown in Figure 5, two approaches were used for identifying which reactants (HNO_3 or NH_3) limited the formation of aerosol nitrate. First, a thermodynamic equilibrium model (SCAPE2) was used to predict aerosol nitrate concentrations after either total ammonia or total nitrate concentrations were reduced. These predictions were compared with current particulate nitrate concentrations to determine the fractional nitrate reduction. Calculations were made for mass reductions of either total nitrate or total ammonia of 10, 20, and 40 percent. Second, excess ammonia was computed for each of the monitoring locations in each database (SCAQS, CADMP, or IMS95, the 1995 Integrated Monitoring Study of particulate formation in the San Joaquin Valley) using the $PM_{2.5}$ size fraction measurements of all inorganic species and the measurements of the gas-phase species, nitric acid and ammonia.

The results indicated that the majority of samples had excess ammonia. Since a fractional nitrate reduction was computed for each sample by running the model with reduced concentrations of either total ammonia ("precursor decreased: NH_3") or total nitrate ("precursor decreased: HNO_3"), the outcomes of the two different precursor reductions may be compared. The model predicted that the majority of samples having positive excess ammonia would show greater reductions of aerosol nitrate if total nitrate were reduced rather than if total ammonia were reduced (Figure 5). The results for 10 and 40 percent reductions of total nitrate or total ammonia were qualitatively similar to those shown in Figure 5 for 20 percent reductions. In all cases, geographical differences were observed, particularly in the SCAQS data. Many of the ammonia-limited samples were from Burbank; in contrast, most of the ammonia-rich samples were from Riverside.